Hindawi
International Journal of Chemical Engineering
Volume 2019, Article ID 9514848, 8 pages
https://doi.org/10.1155/2019/9514848

Research Article

Breakup of the Water Sheet Formed by Two Liquid Impinging Jets

Yakang Xia, Lyes Khezzar, Shrinivas Bojanampati, and Arman Molki

Khalifa University of Science and Technology, P.O. Box 127788, Abu Dhabi, UAE

Correspondence should be addressed to Lyes Khezzar; lyes.khezzar@ku.ac.ae

Received 6 November 2018; Revised 29 December 2018; Accepted 10 January 2019; Published 3 February 2019

Academic Editor: Donald L. Feke

Flow visualization experiments are carried out to study the flow regimes and breakup length of the water sheet generated by two impinging liquid jets from an atomizer made of two identical tubes 0.686 mm in diameter. These experiments cover liquid jet Reynolds numbers based on the pipe diameter in the range of 1541 to 5394. The effects of the jet velocities and impingement angle between the two jets on the breakup performance are studied. Four spray patterns are recognized, which are presheet formation, smooth sheet, ruffled sheet, and open-rim sheet regimes. Water sheet breakup length is found to be consistent with previous experimental and theoretical results in the lower Weber number (based on water jet diameter and velocity) range. In the relatively high Weber number range, the breakup length tends to a constant value with increasing Weber number, and some discrepancies between experimental and theoretical predictions do exist. Measured water sheet area increases with increasing liquid jet Reynolds numbers and impingement angle within the range of the current study.

1. Introduction

Impinging jets configuration refers to two identical oblique liquid jets contained in one plane, which impinge onto each other. Subsequently, a liquid sheet is formed in a plane perpendicular to that containing the liquid jets which can later on atomize and generate liquid droplets. Due to the fact that the dynamic head of one jet contributes to the disintegration of the other jet, impinging jets give rise to good atomization and mixing. Such type of impinging jet atomizers are easy to manufacture and are used in several applications such as rocket propulsion engines and chemical reactors. The characteristics of flow and structure of impinging jets depend on several parameters such as liquid jet velocity and diameter, impingement angle, preimpingement length, and surrounding medium.

Impinging jets have been the subject of several theoretical and experimental studies directed towards the sheet shape, breakup length, sheet and rim thickness, spray patterns, and breakup mechanism. Ryan et al. [1] conducted a theoretical and experimental study of the atomization characteristics of the water sheet generated from the impingement jets using the antisymmetrical wave-based and linear stability-based models for low and high Weber number regimes, respectively. Results indicated that the jet exit conditions strongly affect the spray formation process. Laminar flow from the tube generates large breakup lengths, while turbulent flow results in much shorter breakup lengths. The breakup length is defined as the length of the water sheet from the edge at azimuthal angle of 0° to that at 180°. The predicted dimensionless breakup length L/D, where D is the jet diameter, was found to overpredict the measured one. The reason was attributed to the assumptions introduced in the derivation of theoretical solutions. Li and Ashgriz [2] derived breakup length and width of liquid sheet based on sheet shape predicted by Ibrahim and Przekwas [3]. Significant deviation between the theoretical prediction and experimental results of the breakup length was found at high Weber numbers typically above 200, where the Weber number is defined as the ratio of inertial force to surface tension force. Inamura and Shirota [4] obtained analytical relations for liquid sheet shape, breakup length, and rim thickness. The theoretically predicted shape was not always perfect, but overall the agreement between measurements and theory was found to be satisfactory. Predicted breakup lengths of liquid sheet can differ because of the choice of the critical value of magnitude of disturbances at which liquid sheet breaks up into ligaments. Zhao et al. [5] investigated

theoretically liquid sheet breakup length and width resulting from the impingement of liquid jets issuing from elliptical nozzles. Theoretical predictions of sheet length and width were in good agreement with experimental results, but the sheet formed by elliptical jets is less stable than that by round jets.

Depending on the Reynolds number or Weber number of the liquid jet and angle between the two jets, different spray pattern regimes can be identified. Bush and Hasha [6] obtained a Re-We map which included seven regimes. Ciezki et al. [7] observed the flow regimes of two impinging jets with different fluids. Several breakup regimes were identified and plotted in a Re-We diagram. They were rim with droplet separation, rimless separation, ligament structure, fully developed pattern, and the ray-shaped structure. Li and Ashgriz [2] and Jung et al. [8] also studied flow structures. Most of the spray patterns identified by different researchers are similar, such as the closed rim regime, open-rim regime, and fully developed regime. However, the previously obtained regime maps differ because of the different experimental conditions of the tests. The exact details of the breakup mechanism of the resulting liquid sheet formed by impingement of two identical jets are still not well understood, and various explanations have been put forward. Heidmann et al. [9] are of the view that the liquid sheet generated from the impinging jets becomes unruffled and breaks up because of the aerodynamic waves on the liquid sheet surface, and that impact waves starting from the impinging point are responsible for the breakup of liquid sheet. Dombrowski and Johns [10] have proposed that breakup of liquid sheet is caused by aerodynamic and hydrodynamic unstable waves, where the former dominate the breakup at higher liquid jet velocities and impinging angles. Li and Ashgriz [2] put forward two breakup scenarios based on capillary instability and Kelvin–Helmholtz instability.

Numerical simulation studies are not as numerous as experimental and theoretical ones due to the complexity of the multiphase flow generated by impinging jets. The multiphase flow with multi scales requires considerable computational resources. Inoue et al. [11] performed simulations with a variant of the level set method. Arienti et al. [12] utilized the formulation of CLSVOF (combined level set and volume-of-fluid). Chen et al. [13] conducted a high fidelity direct numerical simulation of impinging jets performance with an improved volume-of-fluid method, which is augmented with adaptive mesh refinement (ARM) techniques. Different levels of mesh refinements were used and spray patterns of liquid chain, closed rim, open rim, unstable rim, and impact waves were obtained from the simulation. This study led to the conclusion that the interaction between the shear layers of the two impinging jets was responsible for the generation of impact waves at impingement point.

It can be seen from the brief literature review that no universally agreed breakup mechanism is available and that differences in the regime map have been observed. The theoretical solutions because of inherent assumptions are limited, and computational studies require a large number of grid points and computational time to obtain sufficiently resolved and reliable results. The present work's objectives include an experimental study using high-speed photography to develop a regime map by identifying breakup regimes and mechanisms of water sheets generated from two liquid impinging jets operating mainly in the turbulent regime over a range of liquid jet velocities or Weber numbers and impingement angles (2θ). The breakup length is also sensitive to the jet exit conditions, and variations in previous measurements have been reported. Consequently, the breakup length is measured and compared against previous experimental studies and existing analytical expressions. Finally, the water sheet area is measured for the first time, as it provides an indication of prestage atomization behavior.

2. Experiment

The closed hydraulic loop used to generate the two impinging jets is illustrated in Figure 1. It consists of a clear acrylic water tank and two magnetically coupled centrifugal pumps, which supply water to the liquid jet pipe nozzles using flexible hoses. Water exiting from the pipe nozzles returns to the water tank. The water flow rate is measured using two Omega FLR1000 ultra-flow sensors separately, which were calibrated with the accuracy of 1%. The flow sensors are connected to an acquisition system programmed in LabVIEW. The temperature of water inside the tank is constantly monitored throughout the experiment using a K-type thermocouple to ensure that it does not affect the fluid viscosity and hence the atomization performance.

The atomizer is made of two stainless steel pipe nozzles of 0.686 mm internal diameter. Each pipe is 152.4 mm in length giving a length to diameter ratio $L_p/D = 220$. It can therefore be assumed that the flow issuing from the pipe exit is fully developed. The two pipe nozzles with sharp edged orifices are positioned on a plate articulated system with a graduated dial that allows a precise positioning and setting of the separation angle between the two water jets within the range from 60° to 120°.

The flow visualization experiment was conducted using a high-speed camera (Photron FASTCAM SA3) operated in background illumination provided by an LED light matrix source. The images were captured and analyzed using the software Photron FASTCAM Viewer Version 352. The resolution pixel was 256×256 at the frame rate of 15,000 fps. Water sheet breakup length and area were obtained from images captured by the high-speed camera. The uncertainty in breakup length caused by random error is estimated to be less than 5% of the measurement, while for water sheet area, it is quite different at various jet velocities, but its maximum value does not exceed 14%.

3. Results

This section discusses the spray patterns, the flow regime map, and the breakup length measurements. Experimental runs were conducted in a range of water jet velocities varying from 2.25 m/s to 7.89 m/s at three impingement angles of 60°, 90°, and 120°. For all of the cases considered, the pre-impingement length was chosen so that it is much smaller

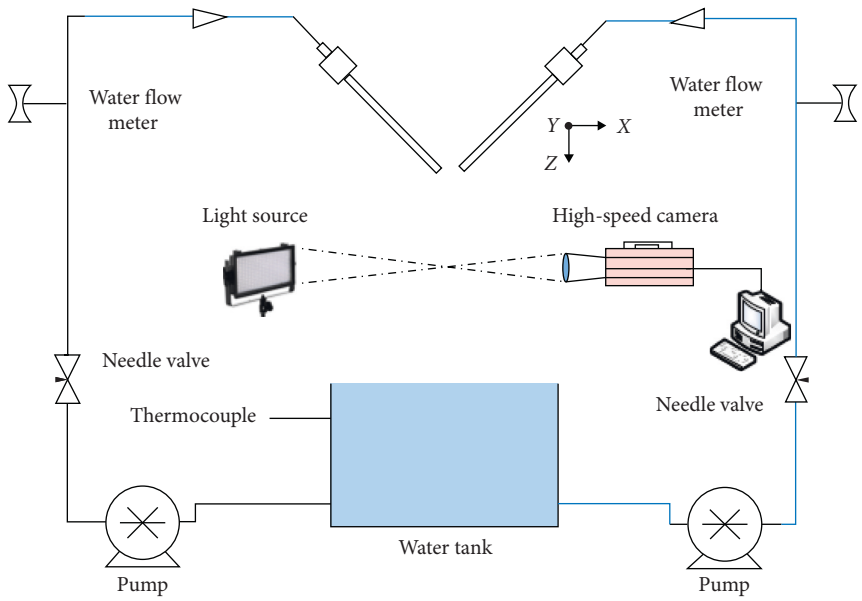

Figure 1: Schematic of experimental setup.

than the jet breakup length. To provide guidance, the geometrical representation and orientation is shown in Figure 2. The plane containing the water sheet is referred to as sheet plane (Y-Z) and the plane perpendicular to it which contains the jets as jet plane (X-Z). For the camera, these will represent the front view (FV) and side view (SV).

Figure 3 illustrates a front view image of the liquid sheet in plane (Y-Z) captured by the high-speed camera. The position where the two water jets impinge onto each other is named as the impingement point. The distance from the impingement point to the tip of the unbroken water sheet is defined as the breakup length.

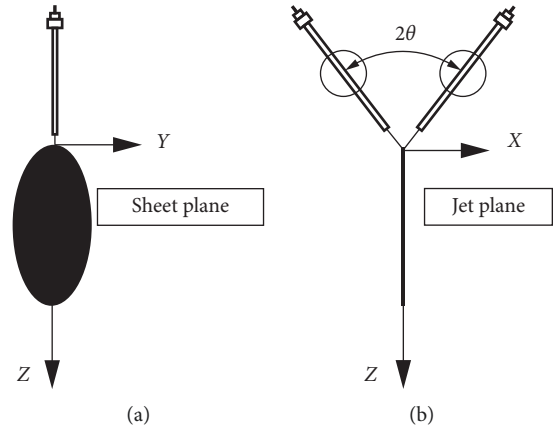

Figure 2: Geometrical orientation of the system. (a) Front view. (b) Side view.

3.1. Spray Patterns. Figure 4 illustrates the flow patterns generated by the two liquid jets at several liquid jet velocities and three separation angles. Two views are recorded for each condition, namely, the front view (Y-Z) and side view (X-Z). It is obvious that the water sheet area increases with the increase of water jet velocities and impingement angle. Four spray patterns are identified from the images captured by the high-speed camera within the current study flow rate range.

3.1.1. Presheet Formation Regime. At small water jet velocities, a small nearly elliptical water sheet is generated, which is bounded by a rim due to the surface tension force. This water sheet is stable but ruffled. However, no ligaments and droplets are generated on the water sheet edge. An irregular and distorted jet is generated from the tip of the water sheet, from which some large droplets are produced due to the growth of surface tension-induced axisymmetric oscillations on the jet surface, which is the jet breakup mechanism in the Rayleigh jet breakup regime as described by Reitz [14]. In Figure 4, the images when the water jet velocities are 2.25 m/s and 3.38 m/s

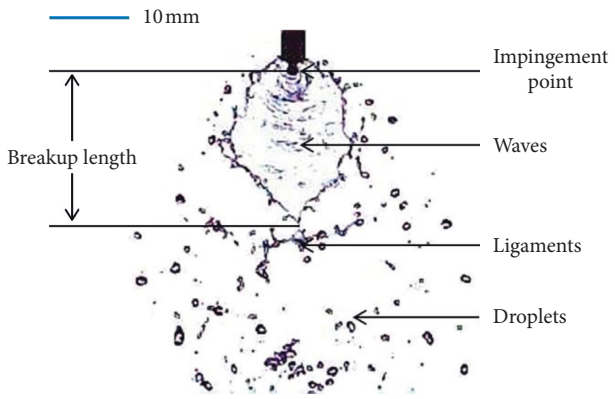

Figure 3: Front view of water sheet (at jet velocity 6.77 m/s and impingement angle 90°).

at an impinging angle of 60° belong to this spray pattern and so do the images at water jet velocity of 2.25 m/s at an impinging angle of 90° and 120° in Figure 4.

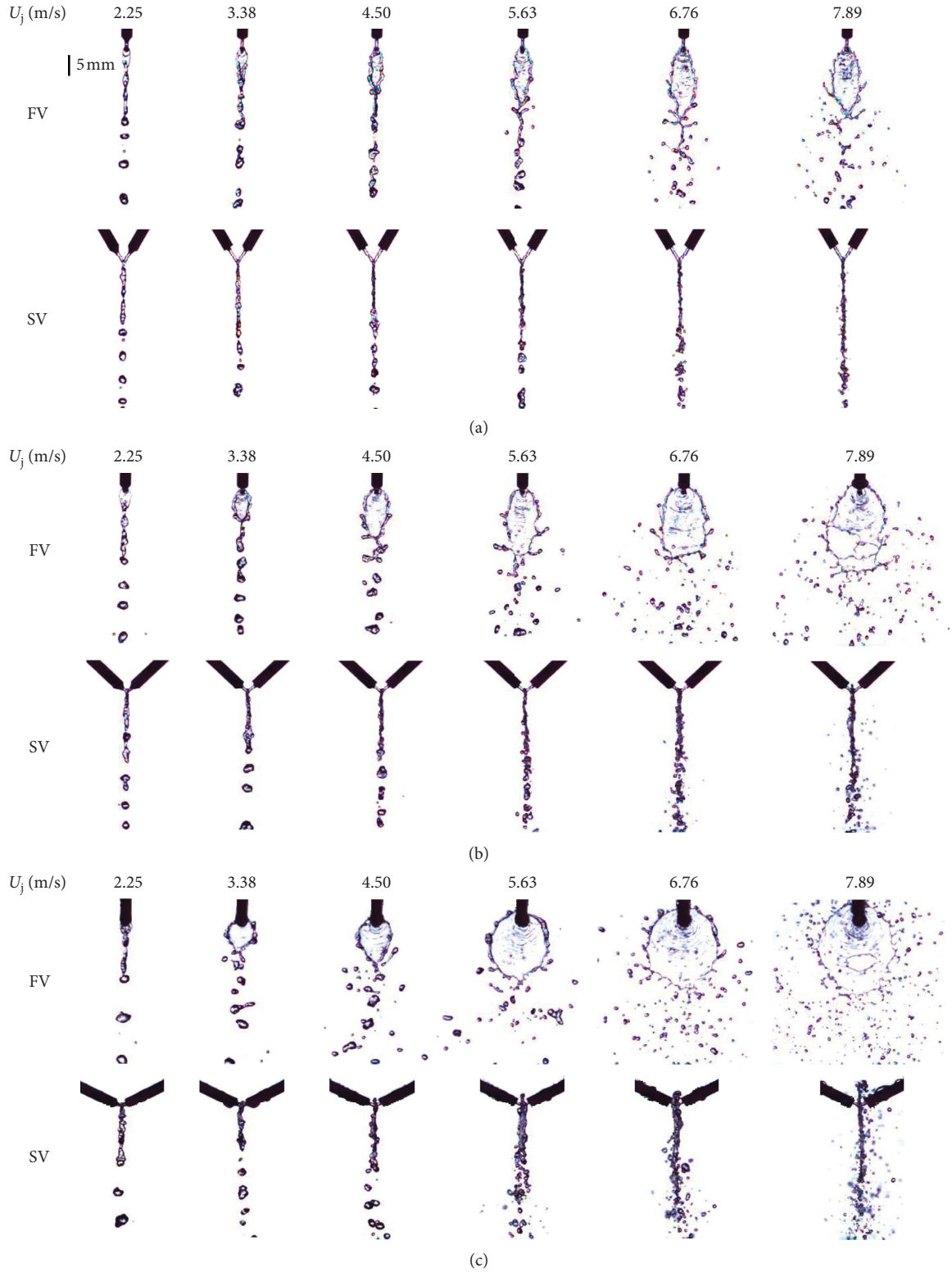

Figure 4: Water breakup structure at different water velocities. FV = front view; SV = side view. (a) $2\theta = 60^\circ$. (b) $2\theta = 90^\circ$. (c) $2\theta = 120^\circ$.

3.1.2. Smooth Sheet Regime. With the increase of water jet velocity, a stable larger and wider water sheet appears, but due to the fact that the momentum force becomes larger than the surface tension force, some droplets appear on the edges of the water sheet and keep developing along the edge until they leave the edge becoming first ligaments and then droplets. The images at water jet velocity of 4.50 m/s and 5.63 m/s at an impinging angle of 60° and the images when the water jets velocities are 3.38 m/s and 4.50 m/s at an impinging angle of 90° and 120° in Figure 4 are of this regime.

3.1.3. Ruffled Sheet Regime. In this regime, also referred to as the unstable regime, surface waves in the sheet are visible from the impingement point. Ligaments and droplets start shedding off the edge of the water sheet due to disturbances from the water jets themselves [15]. The images when the water jet velocities are 6.77 m/s and 7.89 m/s at an impinging angle of 60° and those when the velocities are 5.63 m/s at the impinging angle of 90° and 120° in Figure 4 belong to this regime.

3.1.4. Open-Rim Sheet Regime. Further increasing the water flow rate, waves move and develop on the water sheet surface, which causes the water sheet to become unstable, and as the waves reach the rear of the water sheet, the lower part of the water sheet breaks up into ligaments and droplets due to the Kelvin–Helmholtz-type instability as explained by Li and Ashgriz [2]. In this case, the rim surrounding the sheet confines the breakup of the water sheet breakups and is open, which is clearly shown on the images when the jet velocities reach or exceed 6.77 m/s at the impinging angle of 90° and 120° in Figure 4. The high-speed photography films actually show the sheet to tear and grow back in a more or less periodic way with random generation of perforations that take place randomly in space and time (see Figure 5). The generation of the majority of the liquid droplets still takes place from the rims surrounding the sheet.

Judging from the images and spray patterns of the water sheet, the breakup mechanism can be explained by the fact that at lower jet velocities before open-rim regime takes place, the liquid sheet generated from the impinging jets becomes ruffled and breaks up because of the aerodynamic waves on the liquid sheet surface, while at higher water jet velocities, impact waves generated from the impingement of the two jets dominate the water sheet breakup.

Figure 6 presents the flow pattern regime map using the relationship between the Reynolds number based on the jet average velocity and diameter and impingement angle. It shows that presheet formation regime happens when the water jet is laminar. In the transitional region, the smooth sheet regime appears. When the jet becomes turbulent, a ruffled sheet takes place. At a higher impingement angle, the onset of a spray pattern is initiated at a lower Reynolds number than that at a smaller impingement angle. Although the present results are similar to those obtained by Li and Ashgriz [2] in the sense that the previous identified regimes are also seen in this work, there are significant differences between the two in terms of the shape of the regime map. The reasons behind this can easily be attributed to differences in the emerging liquid jet conditions which are known to strongly affect the spray formation process and hence the flow type obtained.

3.2. Breakup Length. The measured breakup length L is discussed in this section and compared with experimental results by Ryan et al. [1] and theoretically calculated breakup lengths using the correlations from Li and Ashgriz [2] and Ryan et al. [1] based on the existing stationary antisymmetric wave-based theory [3] and linear stability-based theory [16]. For low Weber regime, the theoretical correlation for breakup length is given as

$$\frac{L}{R\mathrm{We}} = \frac{\beta\left(e^{\beta}\sin^2\theta + 1\right)}{4\left(e^{\beta} - 1\right)S}, \tag{1}$$

where β is a coefficient that can be obtained from $\cos\theta = (e^{\beta}+1)/\left\{(e^{\beta}-1)[1+(\pi/\beta)^2]\right\}$; R is the jet radius; θ is half of impingement angle; and We is the Weber number defined as $\mathrm{We} = \rho_{\mathrm{L}} v_{\mathrm{j}}^2 D/\sigma_{\mathrm{L}}$, of which ρ_{L} is the liquid density, v_{j} is the jet average exit velocity, and D is the liquid jet diameter.

For the high Weber number regime, the water sheet breakup length correlation is given as

$$\frac{L}{D} = 5.451\left(\frac{\rho_{\mathrm{a}}}{\rho_{\mathrm{L}}}\right)^{-2/3}\left[\mathrm{We}\, f(\theta)\right]^{-1/3}, \tag{2}$$

where $f(\theta) = [(1-\cos\theta)^2/\sin^3\theta]$, ρ_{a} is the density of air, and ρ_{L} is the density of water.

The measured breakup length at various water jet velocities and impingement angles is obtained by taking the average length from 50 images from the high-speed camera images record to minimize random errors. As shown in Figure 7, the nondimensional breakup length in the laminar case (one single point in the present experiments) does not change much with impingement angle, and it is in agreement with the theoretical solution. Because of the limited number of experimental values obtained at low Weber number in the present work, this conclusion is therefore to be taken with caution. In the turbulent cases, the breakup length firstly increases with the Weber number and then seems to tend towards a constant value at an impingement angle of 120°. Breakup length is found to decrease with increasing impingement angle due to the fact that the momentum perpendicular to the axis increases, which gives a higher impact pressure and shortens the water sheet. Differences between theoretical and experiment values are partly due to the simplifying assumptions embedded in the theoretical correlation which ignore some real effects such as leaving out the dilatational waves [1] and the fact that the ignored jet exit conditions have a significant effect on the breakup behavior. Turbulence present in the jet shear layers is another parameter that can certainly have an effect but has not so far been quantified in a systematic way.

Similarly to the theoretical results of equation (1) shown in Figure 7, the dimensionless breakup length is linearly proportional to the parameter $\mathrm{We}(1-\cos\theta)^2/\sin^3\theta$, and the limited experimental data from the current study are in agreement with it and extend the laminar case by Ryan et al. [1]. When the parameter $\mathrm{We}(1-\cos\theta)^2/\sin^3\theta$ is larger than about 20, the measured results are significantly lower than the theoretical predictions in magnitude, but do, however, follow a similar trend in which both increase with the Weber number.

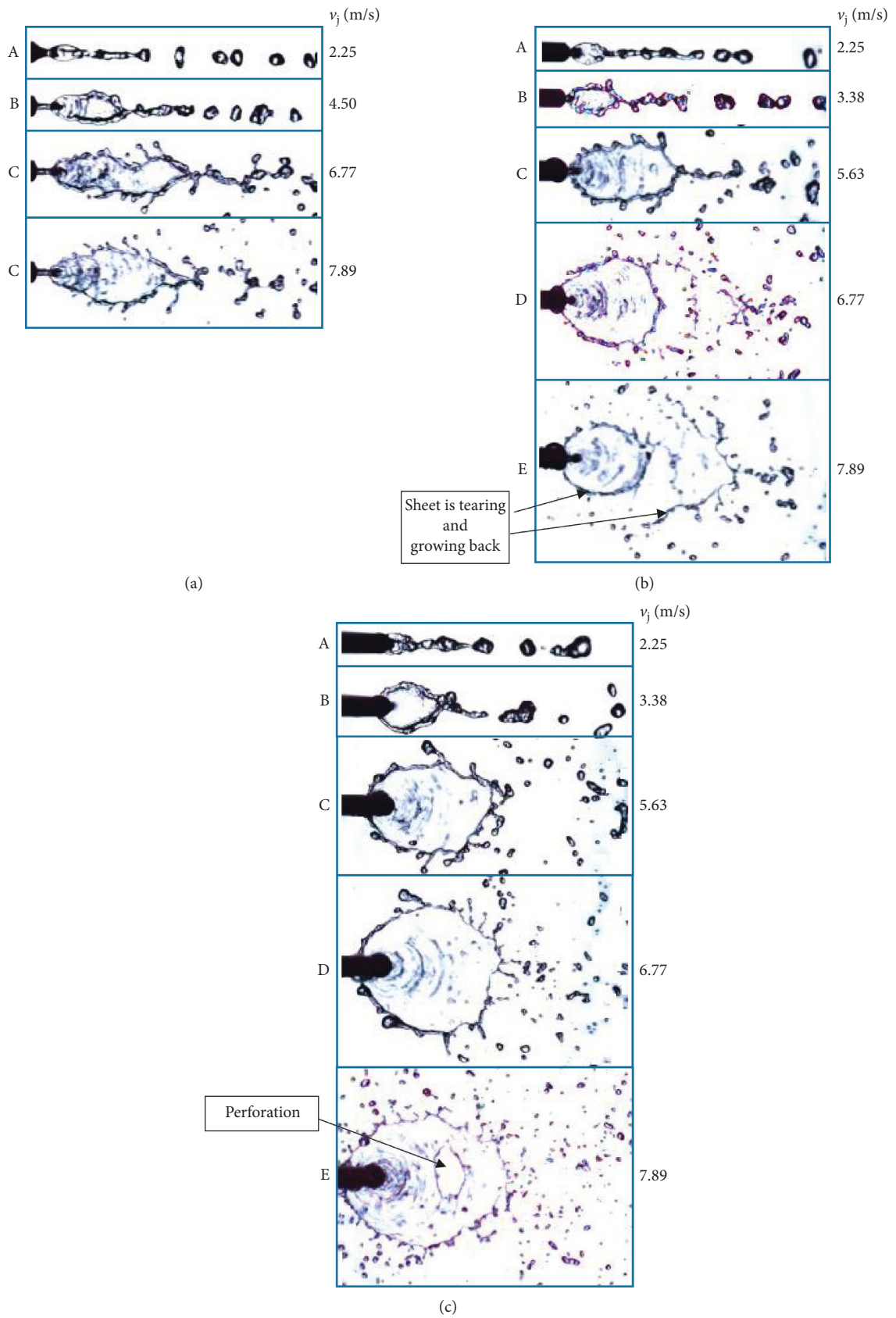

Figure 5: Water sheet structures at different water jet velocities. (A) Presheet formation regime; (B) smooth sheet regime; (C) ruffled sheet regime; (D, E) open-rim sheet regime. (a) $2\theta = 60^{\circ}$. (b) $2\theta = 90^{\circ}$. (c) $2\theta = 120^{\circ}$.

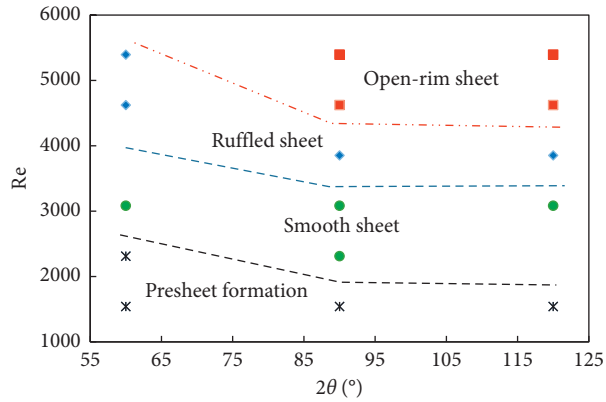

Figure 6: Relationship among breakup regimes in (Re, 2θ) plane.

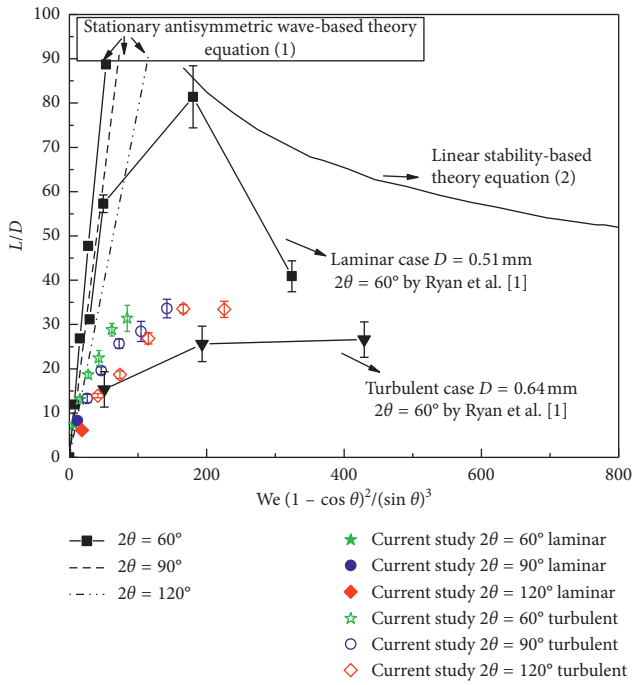

Figure 7: L/D plotted as a function of $\mathrm{We}(1-\cos\theta)^2/(\sin\theta)^3$ (present study used diameter $D = 0.686$ mm).

The origin of the significant deviation between the present experimental results and the theoretical prediction from the equations given earlier in the text at the higher Weber number range is difficult to trace. Nonetheless, possible sources of the discrepancies might be traced to the inherent assumptions used in the linear stability-based theory as highlighted by Inamura and Shirota [4] and the fact that the liquid sheet does not maintain a closed rim when the Weber number of the jets are relatively higher. In addition, the very small, but finite, fluctuation of the water jets' velocity may also account for the observed deviation.

3.3. Water Sheet Area. The water sheet area is defined as the area which is occupied by the unbroken water sheet surrounded by the rim. This is illustrated for several jet exit velocities and impingement angles, i.e., for sheet regimes in Figure 5. The areas were measured using ImageJ [17], and for each case, a sample of 50 images was processed.

The variation of the measured water sheet area with a single jet Reynolds number and the three impingement angles considered is shown in Figure 8. It can be seen that in general and for a fixed impingement angle, the water sheet area increases with water jet exit Reynolds number. The increase is not monotonic; however, all the three curves display a kink at around a value of the Reynolds number equal to 3000. Below and above this value, the rate of change of the area with Reynolds number is linear with a higher rate above 3000. Beyond 3000, the area can increase by up to 350%. This variation with Reynolds number is due to the high pressure generated at impact, which pushes water to spread outwards, resulting in wider water sheets and larger water sheet area, though the sheet length is becoming shorter. This trend of behavior in the sheet area is consistent with the results of Li and Ashgriz [2] who observed a simultaneous but different increase of breakup length and width of water sheet with increasing water jet velocity. However, Inamura and Shirota [4] observed an opposite trend where the area of water sheet decreases with increasing jet velocity when the Reynolds number is larger than 7000 due to the fact that the water sheet is in a flapping sheet regime at the corresponding velocity range, and disintegration of water sheet keeps developing with the increase of jet velocity. The water sheet area increases also with impinging angle. The increase is manifested beyond the Reynolds number value of 3000, whereas it is not large below. Thus, large impingement angles lead to large increases in the area for a particular Reynolds number. This result confirms yet again that impinging angle does have an influence on the lateral spread of the water sheet.

4. Conclusions

An experimental study was conducted to investigate the flow regimes and breakup length for two liquid impinging jets over a range of liquid flow rates. Within the range of flow rates investigated and in agreement with previous findings, four breakup regimes were identified; these are presheet formation, smooth sheet, ruffled sheet, and open-rim sheet regimes. The spatial extent of these regimes on the map was found to differ somehow from previous works. This could be traced back to several effects such as the nozzle geometry and surroundings which are known to influence in intricate ways the breakup regime.

The breakup length was measured for several jet Weber number and impingement angle combinations. The present values are slightly higher than the measured ones by Ryan et al. [1] and lower than theoretical predictions.

Within the range of Reynolds number and impingement angle considered, the area of water sheet was found to increase linearly with Reynolds number with a kink in the curve around a value of Reynolds number of 3000. The area also increases with impingement angle.

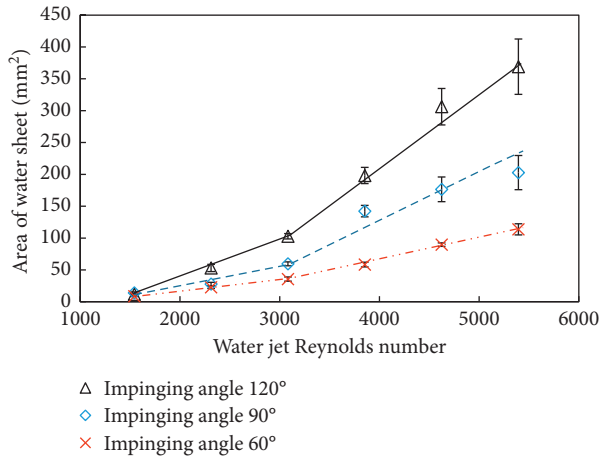

Figure 8: Water sheet area at different water jet Reynolds numbers and impinging angles.

Data Availability

The data used to support the findings of this study are available from Yakang Xia upon request.

Conflicts of Interest

The authors declare that there are no conflicts of interest regarding the publication of this paper.

Acknowledgments

The authors thank the Petroleum Institute, Khalifa University of Science and Technology, for the support.

References

[1] H. M. Ryan, W. E. Anderson, S. Pal, and R. J. Santoro, "Atomization characteristics of impinging liquid jets," *Journal of Propulsion and Power*, vol. 11, no. 1, pp. 135–145, 1995.

[2] R. Li and N. Ashgriz, "Characteristics of liquid sheets formed by two impinging jets," *Physics of Fluids*, vol. 18, no. 8, article 087104, 2006.

[3] E. A. Ibrahim and A. J. Przekwas, "Impinging jets atomization," *Physics of Fluids A: Fluid Dynamics*, vol. 3, no. 12, pp. 2981–2987, 1991.

[4] T. Inamura and M. Shirota, "Effect of velocity profile of impinging jets on sheet characteristics formed by impingement of two round liquid jets," *International Journal of Multiphase Flow*, vol. 60, pp. 149–160, 2014.

[5] F. Zhao, L.-j. Yang, C.-j. Mo, and X.-d. Li, "Characteristics of sheet formed by collision of two elliptical jets at short impact distance," *Journal of Fluids Engineering*, vol. 138, no. 5, article 051201, 2016.

[6] J. W. M. Bush and A. E. Hasha, "On the collision of laminar jets: fluid chains and fishbones," *Journal of Fluid Mechanics*, vol. 511, pp. 285–310, 2004.

[7] H. Ciezki, T. Tiedt, J. V. Kampen, and N. Bartels, "Atomization behavior of Newtonian fluids with an impinging jet injector in dependence upon Reynolds and weber numbers," in *Proceedings of 41st AIAA/ASME/SAE/ASEE Joint Propulsion Conference & Exhibit*, p. 4477, Tucson, Arizona, July 2005.

[8] S. Jung, S. D. Hoath, G. D. Martin, and I. M. Hutchings, "Atomization patterns produced by the oblique collision of two Newtonian liquid jets," *Physics of Fluids*, vol. 22, no. 4, article 042101, 2010.

[9] M. F. Heidmann, R. J. Priem, and J. C. Humphrey, *A Study of Sprays Formed by Two Impinging Jets*, NACA, Washington, DC, USA, 1957.

[10] N. Dombrowski and W. R. Johns, "The aerodynamic instability and disintegration of viscous liquid sheets," *Chemical Engineering Science*, vol. 18, no. 3, pp. 203–214, 1963.

[11] C. Inoue, T. Watanabe, and T. Himeno, "Study on atomization process of liquid sheet formed by impinging jets," in *Proceedings of 44th AIAA/ASME/SAE/ASEE Joint Propulsion Conference & Exhibit*, p. 4847, Hartford, CT, USA, July 2008.

[12] M. Arienti, X. Li, M. C. Soteriou, C. A. Eckett, M. Sussman, and R. J. Jensen, "Coupled level-set/volume-of-fluid method for simulation of injector atomization," *Journal of Propulsion and Power*, vol. 29, no. 1, pp. 147–157, 2012.

[13] X. Chen, D. Ma, V. Yang, and S. Popinet, "High-fidelity simulations of impinging jet atomization," *Atomization and Sprays*, vol. 23, no. 12, pp. 1079–1101, 2013.

[14] R. D. Reitz, *Atomization and other breakup regimes of a liquid jet*, Ph.D. thesis, Princeton University, Princeton, NJ, USA, 1978.

[15] N. Bremond and E. Villermaux, "Atomization by jet impact," *Journal of Fluid Mechanics*, vol. 549, no. 1, pp. 273–306, 2006.

[16] W. Anderson, H. Ryan, S. Pal, and R. Santoro, "Fundamental studies of impinging liquid jets," in *Proceedings of 30th Aerospace Sciences Meeting and Exhibit*, p. 458, Reno, NV, USA, January 1992.

[17] C. A. Schneider, W. S. Rasband, and K. W. Eliceiri, "NIH Image to ImageJ: 25 years of image analysis," *Nature Methods*, vol. 9, no. 7, pp. 671–675, 2012.